•环境工程•

DOI:10.12454/j.jsuese.202300788

本刊网刊

中空碳球负载铋电极CO_2电化学还原产甲酸性能

任明叶[1],韩世豪[1],胡靖斌[1],赵　坤[2],高　攀[3],杨少霞[1*]

(1.华北电力大学 水利与水电工程学院,北京 102206;2.华北电力大学 环境科学与工程学院,北京 102206;3.华北电力大学 新能源学院,北京 102206)

摘　要:二氧化碳电化学还原(Carbon dioxide electrochemical reduction, CO_2RR)在缓解CO_2引起的环境问题和实现产品增值方面前景突出。甲酸是重要的储氢材料和化工中间体,并且CO_2RR产甲酸可以在温和的条件进行,因而受到了广泛的关注。针对CO_2RR活性低、产甲酸速率低的问题,本文采用模板法制备了中空纳米碳球负载氧化铋催化剂(Bi_2O_3@HCS)用于CO_2RR产甲酸。通过扫描电子显微镜(SEM)、透射电镜(TEM)、X射线衍射仪(XRD)和X射线光电子能谱仪(XPS),对Bi_2O_3@HCS催化剂的表面形貌和结构组成进行了分析;采用线性扫描伏安曲线(LSV)和电化学阻抗谱(EIS)电化学测试方法比较了Bi_2O_3@HCS催化剂的电子转移能力。在“H”形电解槽中,研究了Bi_2O_3@HCS催化剂用于CO_2RR产甲酸性能,考察了Bi负载量、阴极电位、$KHCO_3$电解液浓度和溶液pH对产甲酸性能的影响。结果表明,尺寸均一的Bi_2O_3@HCS催化剂在Bi负载量为2.0 mmol/L时,Bi_2O_3@HCS-2催化剂具有最佳的电子转移能力;阴极电位为–1.1 V vs. RHE和电解液浓度为0.1 mol/L $KHCO_3$的条件下,Bi_2O_3@HCS-2催化剂反应2 h甲酸产率可达1 108.11 μmol/L/h/cm^2,其甲酸法拉第效率(F_E)可达50%以上,并且Bi_2O_3@HCS-2催化剂在CO_2RR产甲酸中表现出良好的电极局部pH适应性和稳定性。具有限域作用的中空纳米碳球有效限制了活性组分Bi^0与Bi_2O_3的团聚,丰富的Bi_2O_3提高了CO_2RR产甲酸的反应动力学,并且Bi^0与Bi_2O_3之间存在的金属价态转变进一步提高了催化剂的电子转移能力,从而实现了高的CO_2RR产甲酸速率。

关键词:二氧化碳;电化学还原;甲酸;铋基催化剂

中图分类号:TQ426　　**文献标志码:**A　　**文章编号:**2096-3246(2025)04-0238-10

CO_2的过度排放导致全球变暖,加剧了温室效应[1–2]。在实现碳减排目标的同时,将CO_2转化为高附加值的化学品,是解决环境问题和能源紧缺问题的一个重要途径,具有环保和经济双重效益[3]。CO_2电化学还原(CO_2RR)具有能量转化效率较高、选择性可控、反应装置可模块化等优点,且可产生一系列经济效益良好的化学品(如甲酸、甲醇、乙烯、乙醇等),因而受到广泛关注[4]。其中,甲酸是最适宜规模化生产的化学品[5],主要表现在:产甲酸仅为2e$^-$转移,能耗较低[6];其次,甲酸作为原材料可以被广泛应用(如可作为燃料电池的优良燃料[7]);此外,甲酸是一种有前景的储氢介质,可储存质量分数为4.35%的氢[8]。

CO_2RR产甲酸的性能主要依赖于催化剂[9]。许多催化剂已被用于CO_2RR产甲酸,包括金属基催化剂[10]、碳基催化剂[11]和金属–有机框架(MOFs)[12]。在这些催化剂中,Pb、In、Sn等材料由于高氧亲和力和低氢亲和力对产甲酸表现出高选择性[13],但毒性高、成本高限制了其应用范围[14]。

地球上含量丰富的Bi金属因成本低、过电位低、甲酸选择性高且毒性低等优点被电化学还原领域深入研究[15–17]。叶片状Bi纳米片[18]、Bi_2O_3@C纳米棒[1]和$Bi_2O_2CO_3$纳米片[19]催化剂已被用于CO_2RR产甲酸,并表现出较高的甲酸法拉第效率(F_E)和较好的甲酸产率,但这些催化剂的长期稳定性有待提高。此外,研究表明,活性组分Bi的形貌显著影响CO_2RR产甲酸的性能。Miao等[20]合成了颗粒状的Bi_2O_3(Bi_2O_3-A)和纳米棒状的Bi_2O_3(Bi_2O_3-B)用于CO_2RR产甲酸;其中,Bi_2O_3-A有更小的Tafel斜率,更快的反应速率和更

收稿日期:2023 – 10 – 07　　**修回日期:**2023 – 12 – 06　　**网络出版日期:**2024 – 03 – 28

基金项目:国家自然科学基金项目(52030003)

作者简介:任明叶(1999—),女,硕士生. 研究方向:电化学治理水中污染物. E-mail: rmy6493@163.com

* **通信作者:**杨少霞,教授,博士. E-mail: yangshaoxia2012@126.com

优异的电催化性能。

相比于金属载体，高比表面积、高导电性的碳材料可组装成多种尺寸和结构，能够改善 Bi 基电极 CO_2RR 产甲酸性能[21–22]。Gong 等[23]制备了以洋葱纳米碳为载体的 Bi/MCNOs 电极，电化学表面积是 Bi 电极的 3.4 倍，表现出比 Bi 纳米电极更高的电流密度，极大改善了 CO_2RR 催化活性。

3 维中空纳米碳球（hollow carbon nanospheres，HCSs）独特的空心结构可以有效抑制纳米颗粒团聚，纳米级的壳厚度以及高比表面积可以加快电子传输，被认为是金属活性组分的理想载体，在电化学储能、催化和电化学传感等领域受到研究者们的广泛关注[24–25]，但尚未见到在 CO_2RR 产甲酸中使用。

本文制备了中空纳米碳球负载氧化铋催化剂（Bi_2O_3@HCS）用于 CO_2RR 产甲酸，研究 Bi 负载量、阴极电位、电解液的浓度及 pH 对 CO_2RR 产甲酸性能的影响。研究结果可为合成高效 Bi 基纳米复合材料 CO_2RR 产甲酸提供帮助。

1　材料和方法

1.1　材　料

四丙氧基硅烷（TPOS，分析纯）、氨水（分析纯）、间苯二酚（分析纯）、五水合硝酸铋（$Bi(NO_3)_2{\cdot}5H_2O$，分析纯）、无水乙醇（分析纯）、甲醛（分析纯）、NaOH（分析纯）均购自麦克林生化科技有限公司。Nafion 溶液（质量分数为 5%）由上海河森电气有限公司提供。CO_2（纯度为 99.999%）和 Ar（纯度为 99.999%）由德阳东诚气体有限公司提供。

1.2　催化剂制备

1.2.1　Bi_2O_3@HCS 催化剂的制备

依次将 2.8 mL 的 TPOS（纯度为 97%）、3.0 mL 氨水（浓度为 25%~28%）和 10.0 mL 超纯水加入到 70.0 mL 无水乙醇中，搅拌 15 min 后，在混合溶液中加入 0.4 g 间苯二酚、$Bi(NO_3)_2{\cdot}5H_2O$ 和 0.56 mL 甲醛溶液（质量分数为 37%），继续搅拌 24 h。之后分别用无水乙醇和超纯水进行抽滤各 3 次，得到的棕黄色固体粉末在 60 ℃真空干燥箱中烘干。干燥后的固体在 Ar 气氛中高温煅烧 4 h（800 ℃、900 ℃和 1 000 ℃），升温速率为 5 ℃/min，然后用 NaOH 溶液（10 mol/L）对煅烧后的样品进行 24 h 刻蚀，去除 SiO_2，最后用无水乙醇和超纯水洗涤并干燥，得到 Bi_2O_3@HCS 催化剂。$Bi(NO_3)_2{\cdot}5H_2O$ 负载量分别为 0、1.0、2.0 和 3.0 mmol，制备得到的催化剂分别命名为 HCS、Bi_2O_3@HCS-1、Bi_2O_3@HCS-2 和 Bi_2O_3@HCS-3。

1.2.2　碳载 Bi_2O_3@HCS 工作电极的制备

称取 5 mg 催化剂依次加入 1.7 mL 超纯水、0.2 mL Nafion 溶液（质量分数为 5%）和 0.1 mL 异丙醇（浓度为 99.5%），对混合溶液超声 30 min 使其分散均匀，将混合溶液均匀涂覆在 2.5 cm^2 碳布表面（1×2.5 cm^2，双面滴加）并晾干。工作电极的催化剂负载量为 2 mg/cm^2。

1.3　分析测试仪器

CHI 760E 型电化学工作站，上海辰华公司；Supra55 型扫描电子显微镜（SEM），德国卡尔蔡司公司；Tecnai F20 型透射电镜（TEM），美国 FEI 公司；D8 Advance X 射线衍射仪（XRD），德国布鲁克公司；Thermo Scientific K-Alpha$^+$ X 射线光电子能谱仪（XPS），赛默飞（中国）科技有限公司；Agilent 5110 型电感耦合等离子发射光谱仪（ICP-OES），美国安捷伦科技有限公司。

1.4　电化学测试

在 CHI 760E 上进行 CO_2RR 电化学性能测试，采用三电极体系，分别以 Pt 片为对电极，饱和银/氯化银（Ag/AgCl）为参比电极，涂有催化剂的碳布为工作电极。在 Nafion 117 质子交换膜分离的“H”形密闭玻璃电解槽中，以 $KHCO_3$ 作为电解液。测试过程中不断搅拌阴极室中的电解液，并将 CO_2 持续输送到阴极室中，反应时间为 2 h[26–28]。线性扫描伏安法（LSV）曲线以 5 mV/s 的测试扫描速率记录在–1.0~1.0 V vs. RHE 的电位窗口。电化学阻抗谱（EIS）测试条件：测试开路电压为–0.8 V vs. RHE，频率范围为 1~106 Hz，振幅为 5 mV。

1.5　产物分析

CO_2RR 结束后，用孔径为 0.22 μm 的滤膜过滤反应溶液；用离子色谱仪（ECO IC，瑞士万通）测定甲酸盐的浓度，流动相为 $NaCO_3$（4.5 mmol/L）和 $NaHCO_3$（0.8 mmol/L）的混合溶液，流速为 1.0 mL/min。

甲酸法拉第效率 F_E 计算如下：

$$F_E = \frac{2nF}{Q} \tag{1}$$

式中：n 为产物甲酸的物质的量，mol；F 为法拉第常数，取值为 96 485 C/mol；Q 为通过电极的总电荷，C。

2　实验结果与讨论

2.1　Bi_2O_3@HCS 催化剂结构表征

2.1.1　形貌分析

使用 SEM 和 TEM 分析催化剂的微观形貌和元素分布。图 1 为不同催化剂的 SEM 图。由图 1 可知，HCS 呈现出表面光滑且规则的球形。Bi 负载后，Bi_2O_3@HCS 催化剂仍保持球形；当 Bi 负载量继续增加到 3.0 mmol 时，纳米球形貌发生轻微的变化。图 2 为 Bi_2O_3@HCS-2 的元素分布图。由图 2 可知，C、O 和 Bi 元素均匀分散在

催化剂上。图 3 为不同催化剂的 TEM 图。由图 3 可知，所制备的催化剂均呈现纳米空心球形；当 Bi 的负载量增加到 2.0 mmol 以上时，催化剂仍然保持球形，但碳层逐渐变薄，活性组分逐渐分散在碳球空腔内部，表明空心纳米碳球的空腔对 Bi 活性组分表现出良好的限域作用。

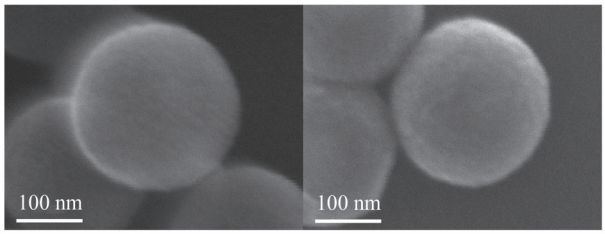

(a) HCS (b) Bi_2O_3@HCS-1

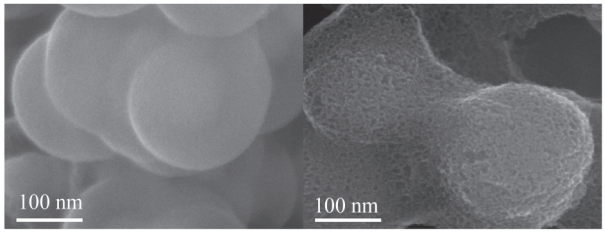

(c) Bi_2O_3@HCS-2 (d) Bi_2O_3@HCS-3

图 1 不同催化剂的 SEM 图

Fig. 1 SEM images of different catalysts

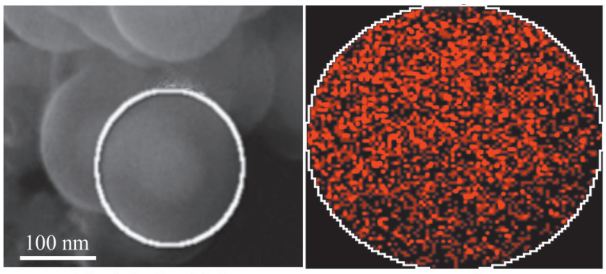

(a) Bi_2O_3@HCS-2 (b) C元素

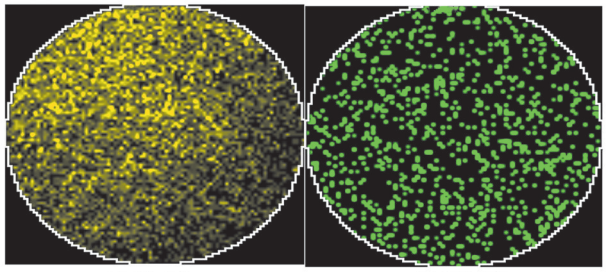

(c) O元素 (d) Bi元素

图 2 Bi_2O_3@HCS-2 的元素分布图

Fig. 2 EDS element mapping images of Bi_2O_3@HCS-2

2.1.2 XRD 分析

为了进一步揭示催化剂的晶体结构，对催化剂样品进行 XRD 分析，不同催化剂的 XRD 图谱如图 4 所示。由图 4 可知，所制备的催化剂均在衍射角（2θ）为 22.5°时出现明显的石墨碳的衍射峰[29]。在 Bi 含量低（1.0 mmol）的 Bi_2O_3@HCS-1 催化剂中，仅出现了微弱的 Bi_2O_3 峰（JCPDS No.27-0050）；随着 Bi 负载量的增加，不仅出现了较强的 Bi_2O_3 衍射峰，还出现了较弱的金属 Bi^0 衍射峰（JCPDS No.85-1329）[28, 30]，说明 Bi_2O_3@HCS-2 和 Bi_2O_3@HCS-3 催化剂中 Bi 以 Bi_2O_3 和 Bi^0 晶体形式共存。由 Scherrer 公式计算得到，活性组分的晶粒尺寸没有明显增大，Bi_2O_3@HCS-2 和 Bi_2O_3@HCS-3 中 Bi_2O_3 晶粒尺寸约为 11 nm，Bi^0 晶粒尺寸约为 1 nm。这主要是因为空心纳米碳球良好的限域作用有效抑制了 Bi 活性组分的团聚，确保了催化剂有较多的活性位点，与 TEM 结果一致。

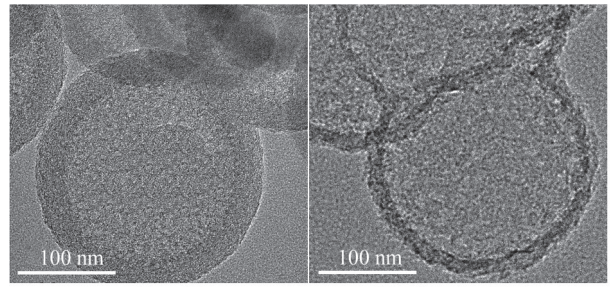

(a) HCS (b) Bi_2O_3@HCS-1

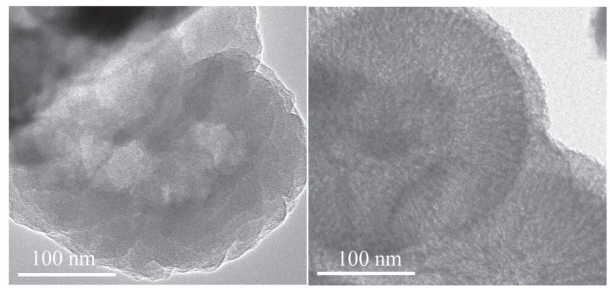

(c) Bi_2O_3@HCS-2 (d) Bi_2O_3@HCS-3

图 3 不同催化剂的 TEM 图

Fig. 3 TEM images of different catalysts

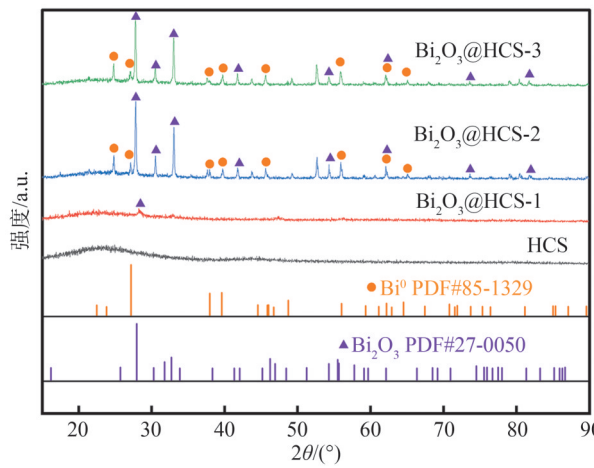

图 4 不同催化剂的 XRD 图谱

Fig. 4 XRD patterns of different catalysts

2.1.3 XPS 分析

利用 XPS 对催化剂表面组成和化合态进行分析，不同催化剂的高分辨率 XPS 能谱和不同催化剂的 Bi 含量分别如图 5 和表 1 所示。

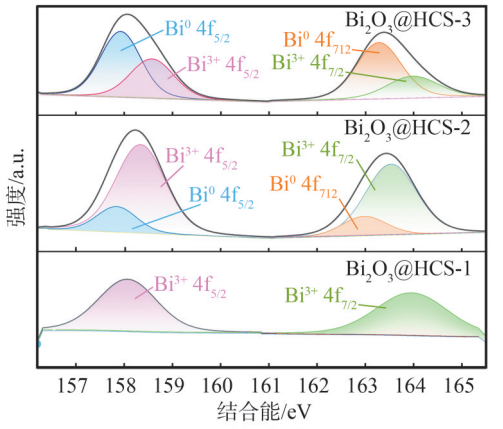

(a) Bi 4f

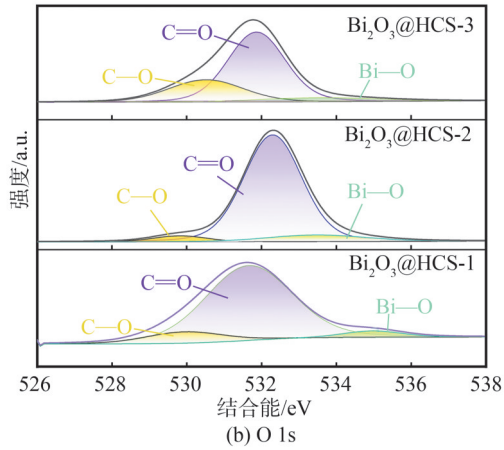

(b) O 1s

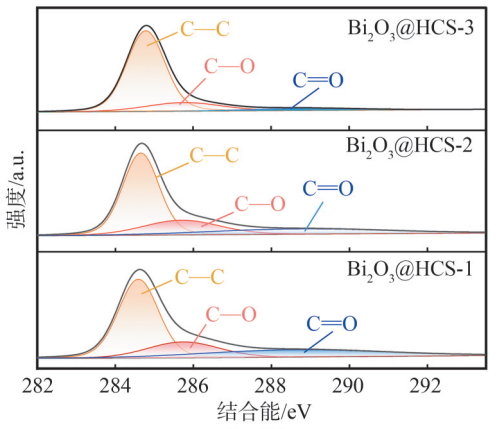

(c) C 1s

图5　不同催化剂的高分辨率XPS能谱图

Fig. 5　XPS spectra of different catalysts

表1　不同催化剂的Bi含量

Tab. 1　Bi content of different catalysts

%

催化剂	Bi^{3+}/C (原子比)①	Bi^0/C (原子比)①	Bi^{3+}/Bi^0 (原子比)①	Bi (质量分数)②
Bi_2O_3@HCS-1	0.08			1.06
Bi_2O_3@HCS-2	0.54	0.46	1.17	18.22
Bi_2O_3@HCS-3	0.48	0.52	0.92	19.17

注：①为XPS测试结果，②为ICP测试结果。

由图5可知，所制备的Bi_2O_3@HCS催化剂均由Bi、O、C这3种元素组成。在Bi 4f的XPS谱图中，159.9、165.3 eV附近出现的特征峰归属于Bi^{3+}，而在158.2、163.4 eV处的特征峰归属于Bi^0。由图5(a)可知，在Bi_2O_3@HCS-1中仅存在Bi^{3+}的特征峰，说明该催化剂仅有Bi_2O_3；在Bi_2O_3@HCS-2和Bi_2O_3@HCS-3中，除了存在Bi^{3+}的特征峰外，还出现了归属于Bi^0的特征峰，表明Bi_2O_3与Bi^0同时存在，与XRD结果一致。

由表1可知，Bi_2O_3@HCS-2具有最高的Bi^{3+}/Bi^0原子比(1.17)，而Bi_2O_3@HCS-3中Bi^{3+}/Bi^0原子比(0.92)低于Bi_2O_3@HCS-2，可能是因为随着Bi负载量的增加，更多的Bi_2O_3得到电子转化成Bi^0。此外，随着Bi负载量的增加，催化剂整体Bi含量呈上升趋势(质量分数从18.22%提高到19.17%)，但是Bi晶粒尺寸没有增加，这也说明活性组分Bi生长于空心碳球内部，从而抑制了活性组分的团聚，此结果与其他文献结果一致[29,31]。O 1s谱图中，在531.8 eV和533.3 eV处有分别归因于C—O键和C═O键的特征峰，在529.9 eV出现了Bi—O的特征峰。从C 1s谱图中可以发现，3种催化剂均在284.8、285.5和288.5 eV出现了3个特征峰，分别对应C—C、C—O和C—O键[32]。

2.2　Bi_2O_3@HCS催化剂电化学活性分析

在Ar和CO_2饱和的$KHCO_3$溶液中使用LSV曲线分析催化剂的CO_2RR电化学活性，结果如图6所示。在CO_2气氛下，与Bi_2O_3@HCS-1相比，Bi_2O_3@HCS-2在−0.60 V vs. RHE附近出现了明显的CO_2还原峰，并且具有更高的电流密度，表明Bi_2O_3@HCS-2催化剂更容易发生CO_2RR[33]，即Bi活性组分的增加有利于吸附和激活CO_2分子，从而提高电极活性[23]。而与Bi_2O_3@HCS-2相比，Bi_2O_3@HCS-3虽然也在−0.25 V vs. RHE附近出现了CO_2还原峰，但电流密度明显下降，这可能是由于Bi^{3+}/Bi^0原子含量比降低，导致催化剂的电子转移能力减弱。

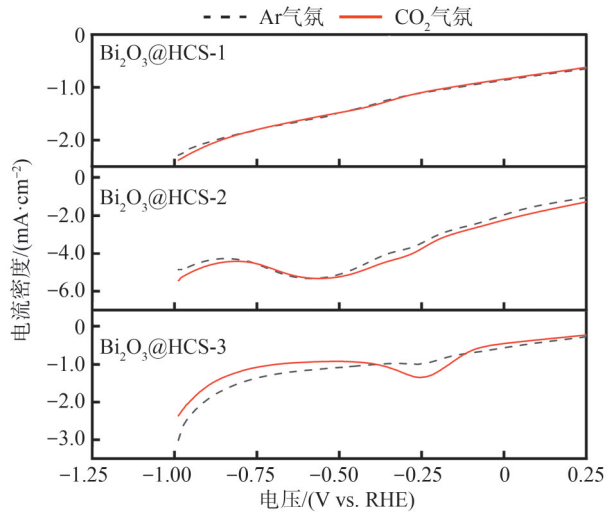

图6　不同催化剂的LSV曲线

Fig. 6　LSV curves of different catalysts

不同催化剂的EIS曲线如图7所示。图7中，Z'和Z''分别为阻抗实部和虚部。由图7可知，Bi_2O_3@HCS催化剂对应的EIS图均呈现半圆形，Bi_2O_3@HCS-2显示出比其他催化剂更小的半圆弧，表明适当的Bi负载有利于加快电极表面的电子转移[34–35]。

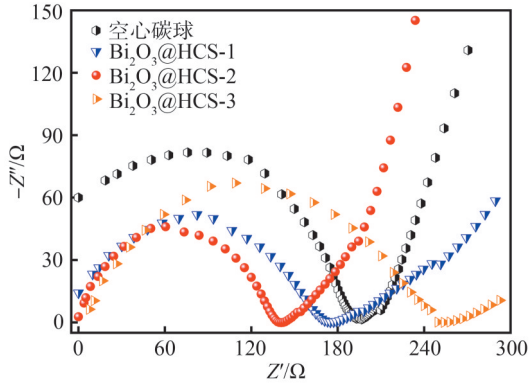

图7 不同催化剂的EIS曲线

Fig. 7 EIS curves of different catalysts

2.3 Bi_2O_3@HCS催化剂CO_2RR甲酸产率的研究

2.3.1 Bi负载量对甲酸产率的影响

图8为不同Bi_2O_3@HCS催化剂的CO_2RR甲酸产率。由图8可知，HCS载体表现出有限的甲酸产率，仅为6.09 μmol/L/h/cm^2；Bi负载后，甲酸产率明显提高。当Bi负载量从1 mmol增加到2 mmol时，甲酸产率从11.97 μmol/L/h/cm^{2}增加到82.31 μmol/L/h/cm^2，但进一步增加Bi负载量时(3 mmol)，甲酸产率降低(54.64 μmol/L/h/cm^2)。

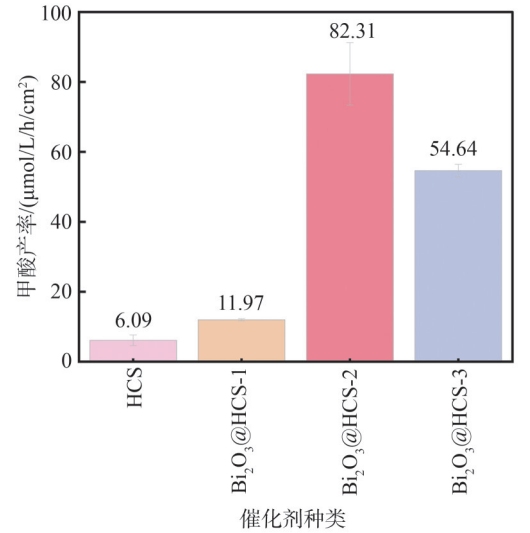

注：反应电位为–0.8 V vs. RHE，电解液$KHCO_3$浓度为0.1 mol/L，pH=6.8。

图8 不同催化剂的甲酸产率

Fig. 8 Formic acid formation rates of different catalysts

图8的结果表明，金属Bi是CO_2RR产甲酸的主要活性组分，Bi_2O_3的含量高有利于吸附和活化CO_2，同时Bi^0和Bi_2O_3在反应过程中可通过金属价态的转变提高电子转移能力，从而获得最高的甲酸产率；但是过量的Bi活性组分会逐渐生长在空心纳米碳球内部，空心纳米碳球的限域作用可以有效抑制活性组分的团聚，但是Bi^{3+}/Bi^0原子比降低，导致电子转移能力下降，故CO_2RR产甲酸速率降低。

2.3.2 阴极电位的影响

以Bi_2O_3@HCS-2工作电极为阴极，研究不同阴极电位条件下甲酸产率和F_E，结果如图9所示。当阴极电位从–0.8 V vs. RHE降低至–1.1 V vs. RHE时，甲酸产率从82.31 μmol/L/h/cm^{2}提高到1 108.11 μmol/L/h/cm^2，F_E可达54.74%，表明Bi_2O_3@HCS-2在较低电位下CO_2RR反应速率良好。当进一步降低阴极电位，甲酸产率逐渐降低，这是因为析氢反应与CO_2RR发生电子竞争，并且析氢反应产生的H_2阻碍了CO_2的传质[36]。

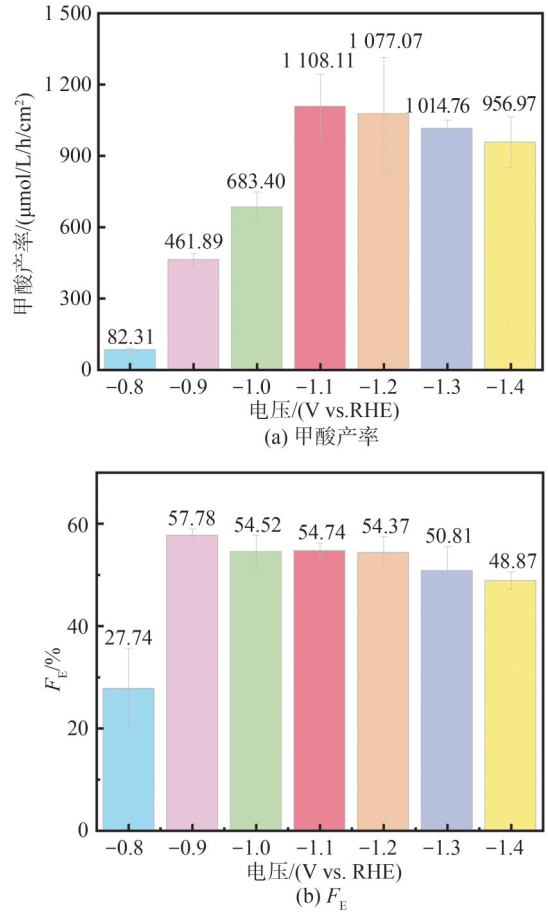

注：电解液$KHCO_3$浓度为0.1 mol/L，pH=6.8。

图9 不同阴极电位下Bi_2O_3@HCS-2催化剂产甲酸性能

Fig. 9 Performance of formic acid formation for Bi_2O_3@HCS-2 catalyst at different cathode potentials

2.3.3 $KHCO_3$电解液浓度的影响

图10为不同$KHCO_3$电解质浓度下Bi_2O_3@HCS-2催化剂CO_2RR的甲酸产率和F_E。由图10可知，$KHCO_3$浓度对CO_2RR产甲酸速率有很大影响。$KHCO_3$浓度为0.1 mol/L时，甲酸产率达到最大值(1 108.11 μmol/L/h/cm^2)，同时实现最高F_E(57.77%)；当$KHCO_3$浓度较低

（<0.1 mol/L）时，溶液中导电离子数减少，使得 CO_2 还原的甲酸产率和 F_E 降低；而当 $KHCO_3$ 浓度较高（>0.1 mol/L）时，会导致电解液黏度增大，阻碍 CO_2 的扩散，并且过多的 HCO_3^- 离子吸附在电极表面，导致活性位点损失，从而限制了 CO_2 电化学还原的进行，降低了甲酸产率和 F_E[37–38]。

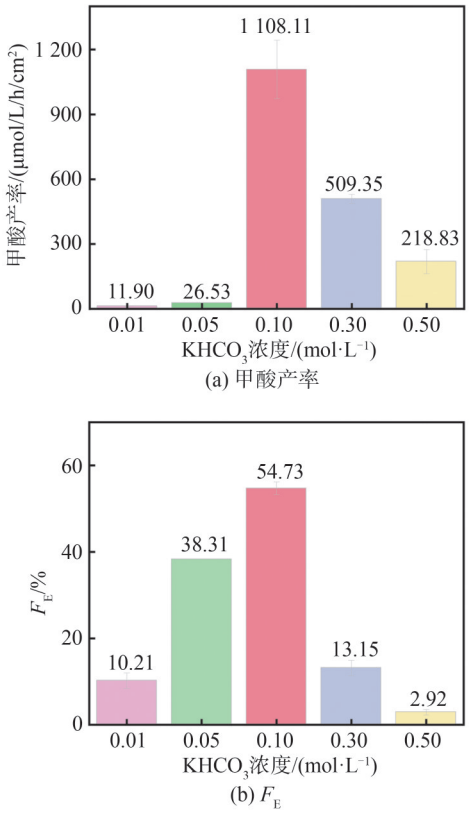

注：反应电位为–1.1 V vs. RHE，pH=6.8。

图 10　不同电解液浓度下 Bi_2O_3@HCS-2 催化剂产甲酸性能

Fig. 10　Performance of formic acid formation for Bi_2O_3@HCS-2 catalyst at different electrolyte concentrations

2.3.4　pH 对甲酸产率的影响

CO_2RR 产甲酸关键中间体的形成和转化受到电极/电解质界面处电解质性质的影响[39–40]。在反应过程中由于 H^+ 不断被消耗，电极附近会出现高浓度的 OH^-，可能会促使 CO_2 转化为惰性碳酸盐。虽然 $KHCO_3$ 具有一定的缓冲能力，但在反应中电极局部 pH 仍明显不同于本体电解质的 pH[41]。因此，选用 pH 缓冲溶液研究 CO_2RR 反应中 pH 值对甲酸产率的影响。

图 11 为不同 pH 缓冲溶液（5.0～8.0）中 Bi_2O_3@HCS-2 催化剂 CO_2RR 的甲酸产率和 F_E。由图 11 可知，在较宽的 pH 范围内甲酸产率和 F_E 并无很大变化。当 pH 从 5.0 升高至 8.0 时，产率仅从 9.82 μmol/L/h/cm² 提高到 40.40 μmol/L/h/cm²，F_E 仅从 0.81% 提高到 4.91%，这表明制备的 Bi_2O_3@HCS-2 催化剂在 CO_2RR 产甲酸中具有较宽的 pH 工作范围[42]。

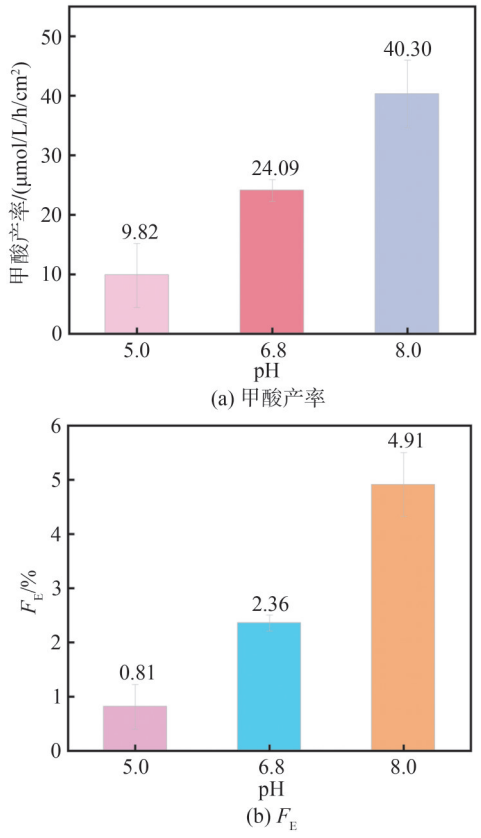

注：反应电位为–1.1 V vs. RHE，电解液 $KHCO_3$ 浓度为 0.1 mol/L。

图 11　不同 pH 条件下 Bi_2O_3@HCS-2 催化剂产甲酸性能

Fig. 11　Performance of formic acid formation for Bi_2O_3@HCS-2 catalyst at different pH

2.4　稳定性分析

图 12 比较了本文 Bi_2O_3@HCS-2 催化剂与其他文献中催化剂 CO_2RR 的甲酸产率。由图 12 可知，本文 Bi_2O_3@HCS-2 催化剂的甲酸产率高于文献报道的相关催化剂[43–47]。

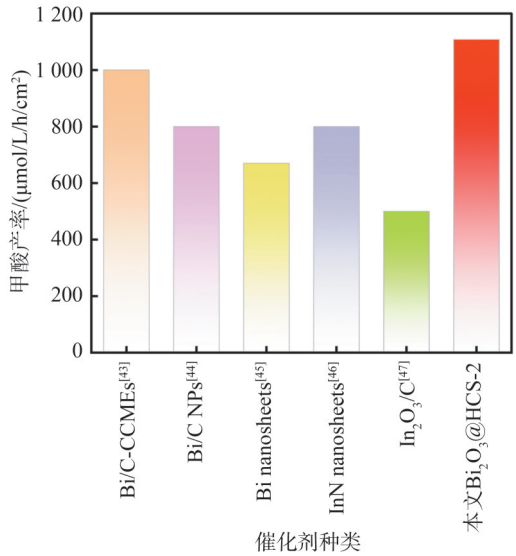

图 12　与已报道催化剂 CO_2RR 甲酸产率的比较

Fig. 12　Comparison of formic acid formation rates in CO_2RR with the reported catalysts

为了考察 Bi_2O_3@HCS-2 催化剂 CO_2RR 产甲酸的稳定性，进行恒电位电解实验，循环反应中甲酸产率如图 13 所示。结果表明，Bi_2O_3@HCS-2 电极经过 5 次循环甲酸产率仍高达 1 090.01 μmol/L/h/cm^2，表现出良好的稳定性。

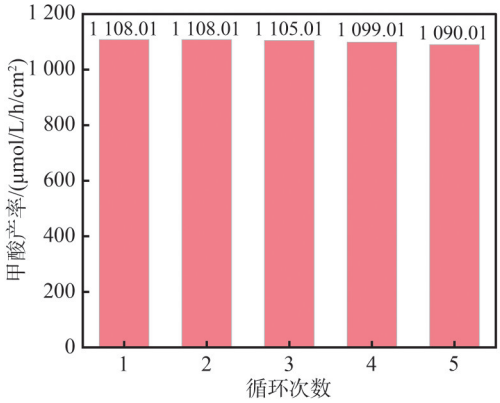

图 13 Bi_2O_3@HCS-2 催化剂 CO_2RR 循环反应中甲酸产率

Fig. 13 Formic acid formation rates in CO_2RR recycle tests with Bi_2O_3@HCS-2 catalyst

3 结 论

本文将中空纳米球状 Bi_2O_3@HCS 催化剂用于 CO_2RR 产甲酸，关键结论如下：

1）具有良好限域作用的中空纳米碳球抑制了 Bi 晶粒尺寸的增加，丰富的 Bi_2O_3 活性位点促进了 CO_2 活化，同时 Bi^0 与 Bi_2O_3 通过价态转变提高了电子转移能力，并且具有最高 Bi^{3+}/Bi^0 原子比的 Bi_2O_3@HCS-2 催化剂表现出最好的 CO_2RR 产甲酸性能。

2）阴极电位、电解液浓度和 pH 均影响 CO_2 电化学还原产甲酸性能。实验结果表明："H"形反应器中，$KHCO_3$ 电解液浓度为 0.1 mol/L、反应点位为−1.1 V vs. RHE 和 pH=6.8 的条件下，Bi_2O_3@HCS-2 催化剂 CO_2RR 的甲酸产率达到 1 108.11 μmol/L/h/cm^2，F_E 为 54.73%；经过 5 次循环，其甲酸产率仍高达 1 090.01 μmol/L/h/cm^2，证明 Bi_2O_3@HCS-2 催化剂具有良好的 CO_2 电化学还原产甲酸性能。

参考文献：

[1] Deng Peilin, Yang Fan, Wang Zhitong, et al. Metal-organic framework-derived carbon nanorods encapsulating bismuth oxides for rapid and selective CO_2 electroreduction to formate[J]. Angewandte Chemie(International Ed), 2020, 59(27):10807–10813.

[2] Ma Wenchao, Xie Shunji, Zhang Xiaguang, et al. Promoting electrocatalytic CO_2 reduction to formate *via* sulfur-boosting water activation on indium surfaces[J]. Nature Communications, 2019, 10(1):892.

[3] Jeffry L, Ong M Y, Nomanbhay S, et al. Greenhouse gases utilization:A review[J]. Fuel, 2021, 301:121017.

[4] Lee J, Kwon Y, Machunda R L, et al. Electrocatalytic recycling of CO_2 and small organic molecules[J]. Chemistry, an Asian Journal, 2009, 4(10):1516–1523.

[5] Wang Qinian, Dong Heng, Yu Hongbing. Fabrication of a novel tin gas diffusion electrode for electrochemical reduction of carbon dioxide to formic acid[J]. RSC Advances, 2014, 4(104):59970–59976.

[6] Senthilkumar P, Mohapatra M, Basu S. The inchoate horizon of electrolyzer designs, membranes and catalysts towards highly efficient electrochemical reduction of CO_2 to formic acid[J]. RSC Advances, 2022, 12(3):1287–1309.

[7] Yu Xingwen, Pickup P G. Recent advances in direct formic acid fuel cells(DFAFC)[J]. Journal of Power Sources, 2008, 182(1):124–132.

[8] Windman T, Zolotova N, Schwandner F, et al. Formate as an energy source for microbial metabolism in chemosynthetic zones of hydrothermal ecosystems[J]. Astrobiology, 2007, 7(6):873–890.

[9] Costentin C, Robert M, Savéant J M. Catalysis of the electrochemical reduction of carbon dioxide[J]. Chemical Society Reviews, 2013, 42(6):2423–2436.

[10] Shinagawa T, Larrazábal G O, Martín A J, et al. Sulfur-modified copper catalysts for the electrochemical reduction of carbon dioxide to formate[J]. ACS Catalysis, 2018, 8(2):837–844.

[11] Wang Hongxia, Chen Yabin, Hou Xiaoli, et al. Nitrogen-doped graphenes as efficient electrocatalysts for the selective reduction of carbon dioxide to formate in aqueous solution[J]. Green Chemistry, 2016, 18(11):3250–3256.

[12] Wang Zhitong, Zhou Yansong, Xia Chenfeng, et al. Efficient electroconversion of carbon dioxide to formate by a reconstructed amino-functionalized indium-organic framework electrocatalyst[J]. Angewandte Chemie(International Ed), 2021, 60(35):19107–19112.

[13] Feaster J T, Shi Chuan, Cave E R, et al. Understanding selectivity for the electrochemical reduction of carbon dioxide to formic acid and carbon monoxide on metal electrodes [J]. ACS Catalysis, 2017, 7(7):4822–4827.

[14] Lei Fengcai, Liu Wei, Sun Yongfu, et al. Metallic tin quantum sheets confined in graphene toward high-efficiency carbon dioxide electroreduction[J]. Nature Communications, 2016, 7:12697.

[15] Tao Yingchu, Wu Shaohui, Zhang Xi. Advances in electrochemical reduction of carbon dioxide[J]. Chemistry, 2001, 64(5):272–277. [陶映初, 吴少晖, 张曦. CO_2 电化学还原研究进展[J]. 化学通报, 2001, 64(5):272–277.]

[16] Gattrell M, Gupta N, Co A. A review of the aqueous electrochemical reduction of CO_2 to hydrocarbons at copper[J].

Journal of Electroanalytical Chemistry,2006,594(1):1–19.

[17] Kopljar D,Inan A,Vindayer P,et al.Electrochemical reduction of CO_2 to formate at high current density using gas diffusion electrodes[J]. Journal of Applied Electrochemistry,2014,44(10):1107–1116.

[18] Yang Jian,Wang Xiaolin,Qu Yunteng,et al.Bi-based metal-organic framework derived leafy bismuth nanosheets for carbon dioxide electroreduction[J]. Advanced Energy Materials,2020,10(36):2001709.

[19] Zhang Yangyang,Chen Yanxu,Liu Rong,et al.Oxygen vacancy stabilized $Bi_2O_2CO_3$ nanosheet for CO_2 electroreduction at low overpotential enables energy efficient CO-production of formate[J].InfoMat,2023,5(3):e12375.

[20] Miao Cancan,Yuan Gaoqing.Morphology-controlled Bi_2O_3 nanoparticles as catalysts for selective electrochemical reduction of CO_2 to formate[J].ChemElectroChem,2018,5(23):3741–3747.

[21] Wu Dan, Huo Ge, Chen Wenyue, et al. Boosting formate production at high current density from CO_2 electroreduction on defect-rich hierarchical mesoporous Bi/Bi_2O_3 junction nanosheets[J]. Applied Catalysis B: Environmental, 2020,271:118957.

[22] Jia Chen, Dastafkan K, Ren Wenhao, et al. Carbon-based catalysts for electrochemical CO_2 reduction[J].Sustainable Energy & Fuels,2019,3(11):2890–2906.

[23] Gong Hao, Wang Yuhong, Guo Yufei, et al. Preparation of Bi/MCNOs electrode and its performance in electrochemical reduction of CO_2[J].Modern Chemical Industry,2022,42(3):144–148. [龚浩,王宇宏,郭雨菲,等.铋/纳米洋葱碳电极的制备及其电化学还原 CO_2 性能研究[J].现代化工,2022,42(3):144–148.]

[24] Xia Xiaohu, Wang Yi, Ruditskiy A, et al. 25th anniversary article: Galvanic replacement: A simple and versatile route to hollow nanostructures with tunable and well-controlled properties[J].Advanced Materials,2013,25(44):6313–6333.

[25] Sun Heng,Qian Junjuan,Yi Yinhui,et al.Synthesis of hollow carbon sphere and its application in electrochemistry [J]. Chemistry, 2017,80(7): 637–641. [孙恒,钱俊娟,易银辉,等.中空碳球合成方法及其电化学应用进展[J].化学通报,2017,80(7):637–641.]

[26] Lee C W,Cho N H,Im S W,et al.New challenges of electrokinetic studies in investigating the reaction mechanism of electrochemical CO_2 reduction[J].Journal of Materials Chemistry A,2018,6(29):14043–14057.

[27] Hatsukade T, Kuhl K P, Cave E R, et al. Insights into the electrocatalytic reduction of CO_2 on metallic silver surfaces[J]. Physical Chemistry Chemical Physics, 2014, 16 (27):13814–13819.

[28] Lee C W,Hong J S,Yang K D,et al.Selective electrochemical production of formate from carbon dioxide with bismuth-based catalysts in an aqueous electrolyte[J].ACS Catalysis,2018,8(2):931–937.

[29] Yang Fa, Elnabawy A O, Schimmenti R, et al. Bismuthene for highly efficient carbon dioxide electroreduction reaction[J].Nature Communications,2020,11(1):1088.

[30] Jiang Yifan,Zhang Xiaodong,Xu Dafu,et al.Efficient three-phase electrocatalytic CO_2 reduction to formate on superhydrophobic Bi–C interfaces[J].Chemical Communications,2021,57(49):6011–6014.

[31] Zhang Dewen,Papaioannou N,David N M,et al.Photoelectrochemical response of carbon dots(CDs) derived from chitosan and their use in electrochemical imaging[J].Materials Horizons,2018,5(3):423–428.

[32] Zhang Zongfei,Yin Haoyong,Zhao Heyu,et al.Preparation of Bi/Bi_2O_3 on porous carbon cuboids for simultaneous determination of dopamine and uric acid[J]. International Journal of Electrochemical Science,2022,17(8):220852.

[33] Guo Qian,Fu Jialong,Zhang Chengyan,et al.Preparation of CoO/RGO@Ni foam electrode and its electrocatalytic reduction of CO_2[J].Journal of Electrochemistry,2021,27(4):449–455. [郭茜,富佳龙,张成燕,等.还原氧化石墨烯@泡沫镍载 CoO 纳米花电极制备及催化 CO_2 性能[J].电化学,2021,27(4):449–455.]

[34] Zhang Zhiyong,Chi Miaofang,Veith G M,et al.Rational design of Bi nanoparticles for efficient electrochemical CO_2 reduction:The elucidation of size and surface condition effects[J].ACS Catalysis,2016,6(9):6255–6264.

[35] Zhang Wenjun, Yang Songyuan, Jiang Minghang, et al. Nanocapillarity and nanoconfinement effects of pipet-like Bismuth@Carbon nanotubes for highly efficient electrocatalytic CO_2 reduction[J].Nano Letters,2021,21(6):2650–2657.

[36] Gabardo C M,O'Brien C P,Edwards J P,et al.Continuous carbon dioxide electroreduction to concentrated multi-carbon products using a membrane electrode assembly[J]. Joule,2019,3(11):2777–2791.

[37] Xu Zhongyu, Zheng Honghe. Research progress on the compatibility of electrolytes with Li-carbon intercalation anodes in lithium-ion batteries Part Ⅱ The relation between electrolyte composition and the compatibility of electrolytes with carbon n[J].Chinese Journal of Power Sources,2000,24(5):295–301. [徐仲榆,郑洪河.锂离子蓄电池碳负极/电解液的相容性研究进展Ⅱ电解液组成与碳负极/电解液的相容性[J].电源技术,2000,24(5):295–301.]

[38] Yuan Shenglun,Ye Dingding,Li Jun,et al.Effects of electrode and electrolyte on the performance of CO_2 electro-

chemical reduction[J]. Journal of Engineering Thermophysics,2016,37(5):1084–1088. [袁圣伦,叶丁丁,李俊,等. 电极及电解液对CO_2电化学还原性能的影响[J]. 工程热物理学报,2016,37(5):1084–1088.]

[39] Gao Dunfeng,Arán–Ais R M,Jeon H S,et al.Rational catalyst and electrolyte design for CO_2 electroreduction towards multicarbon products[J].Nature Catalysis,2019,2(3):198–210.

[40] Moura de Salles Pupo M, Kortlever R. Electrolyte effects on the electrochemical reduction of CO_2[J].Chemphyschem, 2019,20(22):2926–2935.

[41] Ge Wangxin, Zhu Yihua, Jiang Hongliang, et al. Research progress on electrolytes for carbon dioxide electroreduction[J].CIESC Journal,2022,73(8):3433–3447. [葛旺鑫,朱以华,江宏亮,等. 二氧化碳电还原的电解质研究进展[J]. 化工学报,2022,73(8):3433–3447.]

[42] Wang Yirong,Yang Ruxin,Chen Yifa,et al.Chloroplast-like porous bismuth-based core-shell structure for high energy efficiency CO_2 electroreduction[J]. Science Bulletin, 2020, 65(19):1635–1642.

[43] Díaz–Sainz G,Alvarez–Guerra M,Solla–Gullón J,et al.Gas–liquid–solid reaction system for CO_2 electroreduction to formate without using supporting electrolyte[J]. AIChE Journal,2020,66(9):e16299.

[44] Díaz–Sainz G, Alvarez–Guerra M, Ávila–Bolívar B, et al. Improving trade-offs in the figures of merit of gas-phase single-pass continuous CO_2 electrocatalytic reduction to formate[J].Chemical Engineering Journal,2021,405:126965.

[45] Li Zaiqi,Gao Yugang,Meng Xiao,et al.In-situ-derived self-selective electrocatalysts for solar formate production from simultaneous CO_2 reduction and methanol oxidation[J].Cell Reports Physical Science,2022,3(7):100972.

[46] Zhang An, Liang Yongxiang, Li Huiping, et al. *In-situ* surface reconstruction of InN nanosheets for efficient CO_2 electroreduction into formate[J].Nano Letters,2020,20(11): 8229–8235.

[47] Wang Zhitong, Zhou Yansong, Liu Dongyu, et al. Carbon-confined indium oxides for efficient carbon dioxide reduction in a solid-state electrolyte flow cell[J]. Angewandte Chemie(International Ed),2022,61(21):e202200552.

Preparation of Hollow Nanocarbon Spheres Supported Bismuth and Electrocatalytic Reduction of CO_2 to Formic Acid

REN Mingye[1], *Han Shihao*[1], *HU Jingbing*[1], *ZHAO Kun*[2], *GAO Pan*[3], *YANG Shaoxia*[1*]

(1.School of Water Resources and Hydropower Engineering, North China Electric Power University, Beijing 102206, China;
2.College of Environmental Science and Engineering, North China Electric Power University, Beijing 102206, China;
3.School of New Energy, North China Electric Power University, Beijing 102206, China)

Abstract: Carbon dioxide electrochemical reduction (CO_2RR) has great prospects in alleviating environmental problems caused by carbon dioxide emissions and achieving value-added products. Among these chemicals, formic acid is suggested to be one of the economically viable products for hydrogen storage material and chemical intermediates. The industrial production of formic acid is an energy-intensive process, so the production of formic acid in CO_2RR under mild conditions has received extensive attention. The production of formic acid in the CO_2RR depends on the development of highly active and selective electrocatalysts. In order to solve the electrocatalysts with low reaction activity, low formic acid formation rate and poor long-term stability in the CO_2RR process, hollow nano-carbon sphere-supported bismuth oxide catalysts (Bi_2O_3@HCS) were prepared by template method. Metallic bismuth (Bi) has preferable HOCO* adsorption energy and hollow nanospheres have a good active component limiting effect. The chemical composition and surface morphology of the Bi_2O_3@HCS catalysts were in detail analyzed by scanning electron microscope (SEM), transmission electron microscope (TEM), X-ray powder diffractometer (XRD), and X-ray photoelectron spectroscopy (XPS). These results showed that the active components Bi^0 and Bi_2O_3 were uniformly dispersed in the hollow carbon nanospheres, and in the Bi_2O_3@HCS-2 catalyst the highest Bi^{3+}/Bi^0 atomic ratio was achived. The sizes of Bi^0 and Bi_2O_3 particles did not change significantly with increasing Bi loading from 2.0 to 3.0 mmol/L. The result was attributed to the confinement effect of hollow carbon nanospheres in the Bi_2O_3@HCS catalysts. The electrochemical capability of Bi_2O_3@HCS catalysts toward electrochemical CO_2 reduction was investigated by Linear sweep voltammograms (LSV) test in phosphate solution (pH=6.8) saturated with CO_2 or Ar. For Bi_2O_3@HCS-2 catalyst, the current density of CO_2 reduction peak is the largest, which indicated that the higher activity of the Bi_2O_3@HCS-2 catalyst was obtained compared with both Bi_2O_3@HCS-1 and Bi_2O_3@HCS-3 in the CO_2RR. Electrochemical impedance spectroscopy (EIS) was performed to investigate the electron transfer capability of the Bi_2O_3@HCS catalysts. The Bi_2O_3@HCS-2 catalyst exhibited a lower charge-transfer resistance, suggesting a more favorable electron transfer during CO_2RR. The performance of Bi_2O_3@HCS catalysts in CO_2RR for producing formic acid was investigated in a H-shaped electrolyzer. The Bi_2O_3@HCS-2 catalyst, with a Bi loading of 2.0 mmol/L, had the highest formic acid formation rate compared to Bi_2O_3@HCS-1 and Bi_2O_3@HCS-3 catalysts (the Bi loading was 1.0 mmol/L and 3.0 mmol/L, respectively). The effects of the reaction operating conditions (cathode potential, $KHCO_3$ electrolyte concentration and pH) on the formation of formic acid were optimized in the CO_2RR over the Bi_2O_3@HCS-2 cata-

lyst. The results showed that the Bi_2O_3@HCS-2 catalyst with uniformly-sized particles showed the highest formic acid formation rate (1 108.11 μmol/L/h/cm^2), and its Faradaic efficiency (F_E) reached 54.73% in the H-type reactor under the condition of cathode potential of –1.1 V vs. RHE and electrolyte concentration of 0.1 mol/L $KHCO_3$. In order to have an insight into the effects of formic acid formation rate under different pH conditions in the CO_2RR over the Bi_2O_3@HCS-2 catalyst, phosphoric acid buffer solution was used as the electrolyte instead of $KHCO_3$. The results showed that the Bi_2O_3@HCS-2 catalyst exhibited good adaptability in the CO_2RR in a wide pH range. In addition, the good stability of the Bi_2O_3@HCS-2 catalyst in CO_2RR for synthesis of formic acid was proved through the five successive cycle experiments. Compared with the formic acid formation rate in the literatures, the Bi_2O_3@HCS-2 catalyst showed good performance for the following reasons: 1) the hollow nanocarbon spheres with nanoconfinement effect inhibited the agglomeration of the active components of Bi^0 and Bi_2O_3 nanoparticles; 2) the abundant Bi_2O_3 particles improved the reaction kinetics for the formic acid formation in the CO_2RR; 3) the transition of the chemical valence state between Bi^0 and Bi_2O_3 further accelerated the electron transfer capacity. This study on the electrochemical CO_2 reduction for producing formic acid over the Bi_2O_3@HCS-2 catalysts provides a contribution for the synthesis of high-efficiency Bi-based nanocatalysts.

Key words: carbon dioxide; electrochemical reduction; formic acid; Bi-based catalyst

（编辑　陈　雪）

引用格式: Ren Mingye, Han Shihao, Hu Jingbing, et al. Preparation of hollow nanocarbon spheres supported bismuth and electrocatalytic reduction of CO_2 to formic acid[J]. Advanced Engineering Sciences, 2025, 57(4): 238–247. [任明叶,韩世豪,胡靖斌,等. 中空碳球负载铋电极 CO_2 电化学还原产甲酸性能[J]. 工程科学与技术, 2025, 57(4): 238–247.]